Hindawi
International Journal of Antennas and Propagation
Volume 2022, Article ID 5664052, 11 pages
https://doi.org/10.1155/2022/5664052

Research Article

Outspacing Planar Phased Arrays for Wireless Communications Infrastructure

B. G. M. van Ark and A. B. Smolders

Department of Electrical Engineering, Eindhoven University of Technology (TU/e), Eindhoven, Netherlands

Correspondence should be addressed to B. G. M. van Ark; b.g.m.v.ark@tue.nl

Received 9 November 2021; Revised 22 February 2022; Accepted 12 March 2022; Published 6 April 2022

Academic Editor: Chien-Jen Wang

The future mobile-data demand, driven by 5G and 6G wireless communications, puts enormous pressure on the required infrastructure. Especially the need for higher data rates and corresponding higher operating frequencies calls for new transmitter concepts with improved power-added efficiencies. Outspacing, which combines outphasing, also known as linear amplification with nonlinear components (LINC), a phased array, and spatial power combining, could be a promising solution for these challenging performance requirements. In this paper, an extended array-level analysis is performed on the efficiency, mutual coupling, and transmit performance of outspacing arrays supported by new performance metrics, since conventional metrics show to be insufficient for analyzing the outspacing concept. The analysis of the concept is performed on two different planar outspacing configurations. The presented outspacing concept with an element spacing of $\lambda_0/2$ appears to be very suited for applications that require a limited scan range, typically smaller than $\pm 20^{\circ}$. A prototype is realized and characterized for a limited-scan scenario at 2.4 GHz to limit technology-related risks in the verification of the outspacing concept. The outspacing planar array is tested using an over-the-air (OTA) test concept applied in an anechoic test facility. An error vector magnitude below 3%, when transmitting a QAM16 signal, is realized in the main beam of the antenna without the use of calibration. Furthermore, an analysis is done on additional efficiency improvements. The active reflection coefficient, which is strongly related to the mutual coupling between the array elements, appears to have very interesting properties for improving amplifier drain efficiency by active load modulation.

1. Introduction

The continuously growing demand for data puts an enormous pressure on the requirements for wireless transceivers. Especially in commercial applications, the increasing data rates have converse effects on key parameters such as energy consumption, size, and weight. Power amplifiers are the workhorses of the wireless transceivers, with linearity and efficiency as key performance metrics. The increasing operating frequency up to and including mm-waves results in an increase in free-space losses. In order to overcome the high free-space losses and achieve sufficient effective isotropic radiated power (EIRP), beamforming antenna systems are required, such as phased arrays with a large number of antenna elements. Furthermore, these phased arrays require a high level of integration between RF electronics and antenna elements in order to reduce losses and overall system costs.

In traditional phased arrays, the transmitter efficiency is mainly determined by the amplifier. These amplifiers, operated generally in a linear class, such as class-(A)B, have poor efficiencies at mm-wave frequencies. They need to be operated at back-off to meet the required EVM and spectral mask specifications. The back-off efficiency can be improved by using a Doherty topology [1], but at mm-waves, this topology suffers from high additional losses and nonideal operation [2]. When amplitude tapering is required, the amplifiers are further reduced in peak power, further reducing the transmitter efficiency.

Outphasing, also known as LINC [3], is one of the promising concepts for meeting the challenging requirements of high data rate and energy efficient wireless

transmission. The concept achieves amplitude modulation by vectorial addition of two or more phased-modulated, constant envelope signals. In this paper, the *outspacing* concept is used, which is an extension of outphasing, where the vectorial addition is performed in free space, reducing additional interconnection losses and components. Apart from the reduction in interconnection losses, the amplifiers can be optimized to operate in full compression and therefore with maximum efficiency instead of linearity. When the mutual coupling of the phased array can be used to achieve load modulation, the outspacing efficiency at back-off can be greatly improved. Also, the amplitude tapering could effectively be done by density tapering or supply modulation without impact on back-off efficiency.

The concept of spatial power combining is not new [4–8], but no extended work is done on the planar outspacing array. In [9], briefly, the impact of the configuration on the performance of a linear outspacing array is shown. Here, we will extend this concept towards planar arrays and we will introduce new performance metrics for analyzing these outspacing systems. The extension to planar outspacing arrays enables the investigation of many different array configurations. Adapting the element grid and outspacing polarity distribution can already have a major impact on the array behavior and performance.

In this paper, the outspacing concept is analyzed in detail by comparing various array configurations, both using simulation models and by experimental verification. Furthermore, new performance metrics to evaluate the performance of the outspacing arrays are introduced. Because of the time-dependent array pattern and signal distortion introduced by the outspacing concept, well-known performance metrics of planar phased arrays cannot be used for evaluating the performance of the outspacing arrays. The time average array pattern is introduced for analyzing the time-dependent radiation pattern when transmitting a complex signal such as using QAM16 modulation. Furthermore, the error vector magnitude as a function of (u, v) coordinates is used for determining the impact of outspacing on the signal quality. The new metrics are used to analyze a regular planar phased array and to investigate various outspacing configurations. In this paper, we will primarily focus on array configurations, which support applications that require a limited scan range, such as in twist and sway compensation in point-to-point communications [10], since the scan range of the outspacing concept is limited to $\pm 20^\circ$ when the default element spacing of $\lambda_0/2$ is used.

This paper is organized as follows: in Section 2, the basic equations for calculating the array performance are described, new performance metrics are introduced, and two configurations and the impact of scanning are analyzed; Section 3 describes the demonstrator design, experimental results, and the influence on the active reflection coefficient; lastly, in Section 4, an outlook is given on the efficiency performance of the outspacing concept and the possible improvements.

2. The Outspacing Phased Array

The basic outspacing concept is illustrated in Figure 1 and is based on the LINC concept proposed by Cox [3]. The array

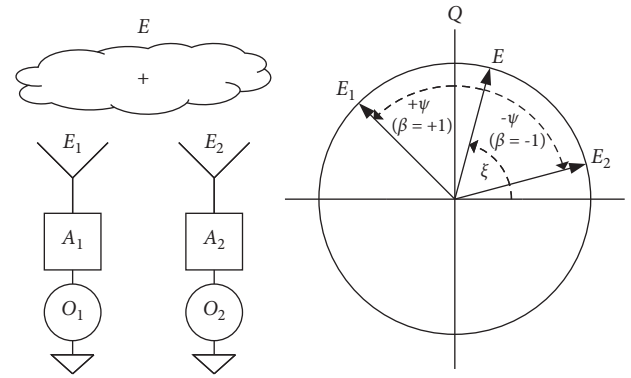

Figure 1: Basic outspacing concept, where amplitude modulation is achieved by vectorial addition of two phase (ψ) modulated signals in space. E is the complex amplitude of the electric field represented in the frequency domain.

consists of at least one antenna pair, where each antenna is driven by its own source. The original signal, a complex vector with an amplitude $r(t)$ and phase $\xi(t)$, is decomposed in two phase-modulated constant envelope signals, O_1 and O_2, where the direction (polarity) of the phase $\psi(t)$ is opposite for both sources. The required outspacing phase $\psi(t)$ can be calculated by $\psi(t) = \arccos(r(t)/r_{\max})$, where $r(t)$ is the instantaneous signal amplitude and $r_{\max}$ is the maximum signal amplitude [11]. By vectorial addition of both phase-modulated signals (E_1 and E_2) in free space, the desired amplitude modulated signal (E) is constructed in the far-field region. A complex excitation coefficient (A) can be added when beam steering and/or amplitude tapering is required.

2.1. The Basic Planar Outspacing Phased Array Equations. The planar array outspacing concept is shown in Figure 2, where only the transmit mode is shown. It is assumed that each antenna-element is fed with its own outphasing source. Optionally, the excitation coefficient for amplitude tapering or beam steering can be added. The element numbering in x and y direction, k and l, respectively, is combined in the element index j according to $j = (l-1)K + k$. The basic equation for calculating the array factor of an outspacing planar array is quite similar to the expression for a linear array, as provided in [9]. The array pattern is calculated in (u, v) coordinates ($u = \sin\theta\cos\varphi$ and $v = \sin\theta\sin\varphi$), which gives us the following expression for the array factor of an outspacing planar array:

$$\vec{F}(u,v) = \sum_{k=1}^{K}\sum_{l=1}^{L} \vec{f}_j(u,v) A_j O_j e^{jk_0\left(p_x u + p_y v\right)}, \tag{1}$$

where $\vec{f}_j(u,v)$ is the element pattern, k_0 is the free-space wavenumber, and A_j is the complex excitation coefficient of element j that provides amplitude tapering ($|a_j|$) and beam steering towards (u_0, v_0):

$$A_j = |a_j| e^{-jk_0\left(p_x u_0 + p_y v_0\right)}, \tag{2}$$

in which p_x and p_y are the element position in x and y direction, respectively. The outspacing vector O_j is found by

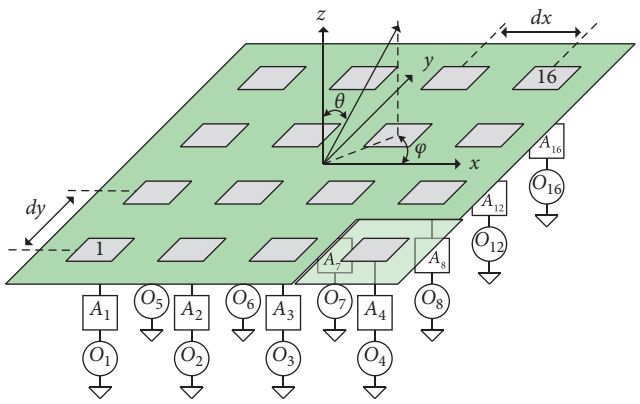

Figure 2: Example of a 4×4 patch antenna outspacing concept.

$$O_j = e^{j\left(\xi + \beta_j \psi\right)}, \tag{3}$$

where ξ represents the angle of the original signal and ψ represents the outphasing angle. The parameter β_j defines the outspacing polarity ($+\psi$ or $-\psi$, respectively) for each specific element and belongs to the set $\beta_j = \{-1, 1\}$. Because the phase ξ and ψ will be equal for all elements, only two outspacing vectors exist, $O(-\beta)$ and $O(+\beta)$.

2.2. Outspacing Array Performance Metrics. In a typical use case in wireless communications, a higher-order modulated signal, such as QAM16, will be transmitted by the array. In case of an outspacing array, this results in a time-dependent array pattern because of the varying outphasing angle ψ. Therefore, we need to use other performance parameters compared to traditional array antenna performance metrics. In order to visualize the array pattern of the planar outspacing array during the transmission of a modulated signal, the time average array pattern (TAAP) is introduced:

$$\overrightarrow{\overline{F}}(u, v) = \frac{\sum_{n=1}^{N} \overrightarrow{F}(u, v, n)}{N}, \tag{4}$$

where $\overrightarrow{F}(u, v, n)$ represents the time-dependent array pattern and n is the timestamp.

Apart from the TAAP, the error vector magnitude (EVM) can be used to describe the signal quality in the (u, v) plane [9]. The RMS value of the EVM will be used [12], which is also the preferred method used by 3GPP [13]. EVM_{RMS} for each point in the uv-plane can be calculated by

$$EVM_{RMS}(u, v) = \frac{\sqrt{(1/M)\sum_{m=1}^{M} \left|S_i(m) - S_r(u, v, m)\right|^2}}{\sqrt{(1/M)\sum_{m=1}^{M} \left|S_i(m)\right|^2}}, \tag{5}$$

where $S_i(m)$ is the ideal transmitted constellation point m and $S_r(u, v, m)$ is the received constellation point m at position (u, v).

In this paper, an QAM16 modulated signal is used with a corresponding peak-to-average power ratio (PAPR) of 6.5 dB. In order to be able to analyze and compare various outspacing array topologies and to apply the new performance metrics, first, the performance of a regular dense array without outspacing is investigated. A regular dense 8×8 array forms the reference case to benchmark the outspacing configurations. The array with $0.5\lambda_0$ element spacing uses an element pattern ($|\overrightarrow{f}_j(u, v)|$) with a $\sqrt{\cos\theta}$ dependence for each element. Since the $\cos\theta$ radiation power pattern does not exist outside the visible space ($|u^2 + v^2| > 1$), the element pattern is fixed at 0.1 ($|\overrightarrow{f}_j(u, v)| = 0.1$) in this region, which results in the following element pattern:

$$\left|\overrightarrow{f}_j(u, v)\right| = \begin{cases} \sqrt{\cos\theta}, & \text{if } \left|u^2 + v^2\right| \le 1, \\ 0.1, & \text{otherwise.} \end{cases} \tag{6}$$

The element pattern is fixed to this artificial value outside the visible space in order to analyze grating lobes in this region, which can become dominant in a scan scenario. The relevant characteristics of a regular array are shown in Figure 3, where the area within the red circle represents the visible space. The figure is normalized at the maximum instantaneous main beam amplitude, which occurs at the outspacing angle $\psi = 0$. This results in a TAAP level of the main beam which is equal to the PAPR of the signal. Furthermore, random noise is added to each element, such that the carrier-to-noise ratio (C/N) [14] is equal to 50 dB. The added noise results in a more realistic system-level behavior, since without this noise, the EVM plot of Figure 3(b) will be constant in all directions at 0%. The peak sidelobe level (PSLL) of the array is −19.7 dB, 13.2 dB lower than the main beam, which is as expected for a regular array with uniform tapering [15]. Apart from the PSLL, the average sidelobe level (ASLL) is calculated by averaging all transmitted signal power inside the visible space, but outside the main beam ($|u| < 0.25 \wedge |v| < 0.25$). This resulted in an ASLL of −35 dB, which is 28.5 dB lower than the main beam. Because of the linear behavior of the regular array, no signal distortion occurs, resulting in an almost constant EVM of 0%, except close to the array pattern zeros, where the noise is dominant.

2.3. Nonsymmetric Outspacing Array Configuration. The most straightforward outspacing configuration, called the nonsymmetric, is shown in Figure 4(a). In the array configuration, the blue tiles represent outspacing coefficients with $\beta_j = +1$ and red elements $\beta_j = -1$. The configuration is called nonsymmetric due to its nonsymmetric β_j distribution over the x and y axes. The TAAP of the nonsymmetric configuration when excited with the QAM16 signal is shown in Figure 4(b). The TAAP in the visible space is very comparable to a regular array, and the maximum PSLL is −19.7 dB, 13.2 dB lower compared to the main beam, which is equal to a regular nonoutspacing planar array. The ASSL of the symmetric configuration is −32.5 dB, which is only 2.5 dB worse compared to a regular dense array. The main difference can be found outside the visible space, where clearly the appearance of grating lobes is visible at $|u| = |v| = 1$. The slightly higher sidelobe level in the visible space can be reduced by using an additional amplitude tapering and by reducing the element spacing. The latter is

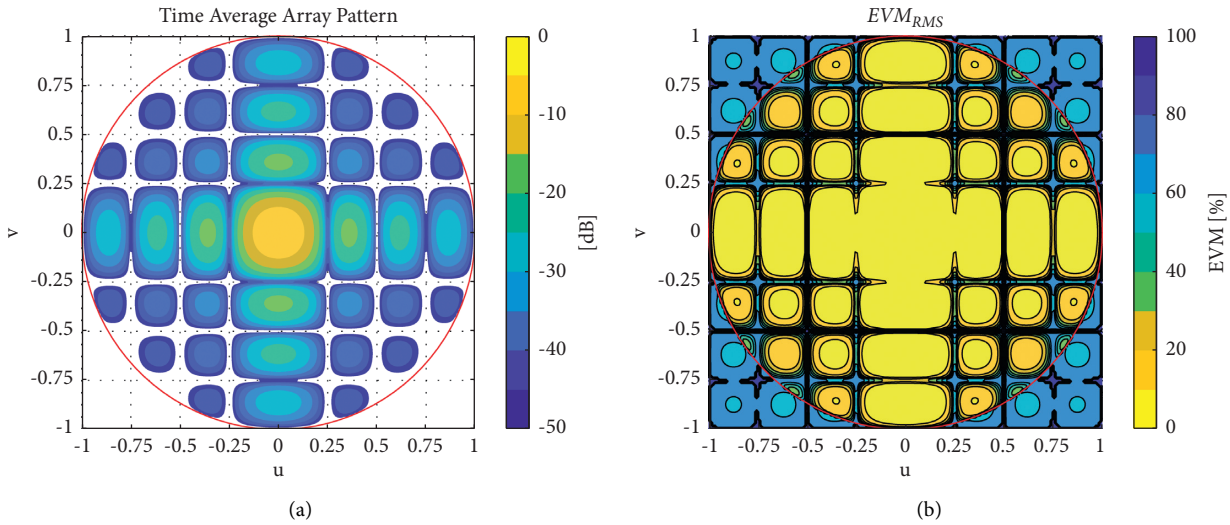

FIGURE 3: Regular (nonoutspacing) array performance: $K = L = 8$, $d_x = d_y = (\lambda_0/2)$, $(C/N) = 50\ dB$, transmitted signal is QAM16, and a $\cos\theta$ element power pattern is used. (a) Time average array pattern. (b) EVM.

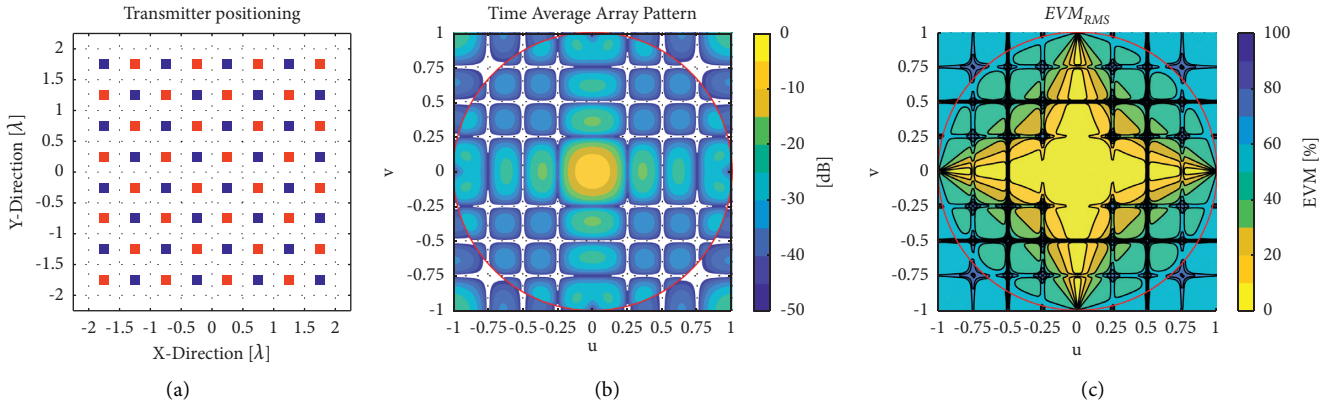

FIGURE 4: Nonsymmetric outspacing array performance: $K = L = 8$, $d_x = d_y = (\lambda_0/2)$, $(C/N) = 50\ dB$, transmitted signal is QAM16, and a $\cos\theta$ element pattern is used. (a) Array configuration. (b) Time average array pattern. (c) EVM.

important when a large scan range is required. The EVM in Figure 4(c) shows strong degradation outside the main beam, especially outside the u and v axes, which is expected and also very beneficial from a security point of view. This is an additional feature of the outspacing concept as compared to traditional arrays.

2.4. Symmetric Outspacing Array Configuration. The symmetric configuration, shown in Figure 5(a), is a logical evolution of the nonsymmetric configuration, where β_j has a symmetric configuration with respect to the x and y axes. The TAAP of the symmetric configuration when excited with the QAM16 signal is shown in Figure 5(b). The main difference which can be observed in the array pattern compared to the nonsymmetric configuration is the reduction of the amount of sidelobes, without increasing the half power beam width of the main beam. The maximum PSLL is −16.6 dB, which is 3.1 dB higher compared to the nonsymmetric configuration. The ASSL is −28 dB and 4.5 dB higher compared to the nonsymmetric configuration, caused by the higher sidelobes. The EVM behavior shown in Figure 5 also shows strong degradation outside the main beam.

2.5. Outspacing Configuration Comparison. The TAAP and EVM performance at the cross section $u = 0$ or $v = 0$ of the regular array and outspacing symmetric and nonsymmetric configuration is very similar. The largest differences in performance can be observed at the center of the four quadrants and especially in the diagonal plane at $\varphi = 45^\circ$. The TAAP and EVM performance at $\varphi = 45^\circ$ is shown in Figure 6. The sidelobes of the symmetric configuration are significantly higher compared to the nonsymmetric configuration, which has a constant sidelobe level at approximately −30 dB. The EVM performance of the three configurations is close to zero within the main beam. Outside the main beam, both outspacing configurations have clearly reduced EVM performance compared to the regular array.

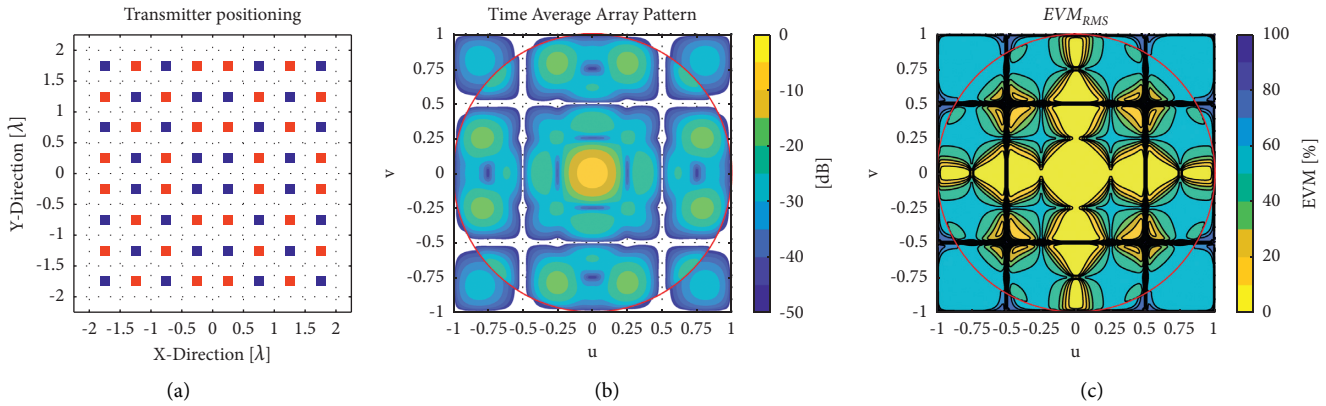

FIGURE 5: Symmetric outspacing array performance: $K = L = 8$, $d_x = d_y = (\lambda_0/2)$, $(C/N) = 50\ dB$, transmitted signal is QAM16, and a cos θ element power pattern is used. (a) Array configuration. (b) Time average array pattern. (c) EVM.

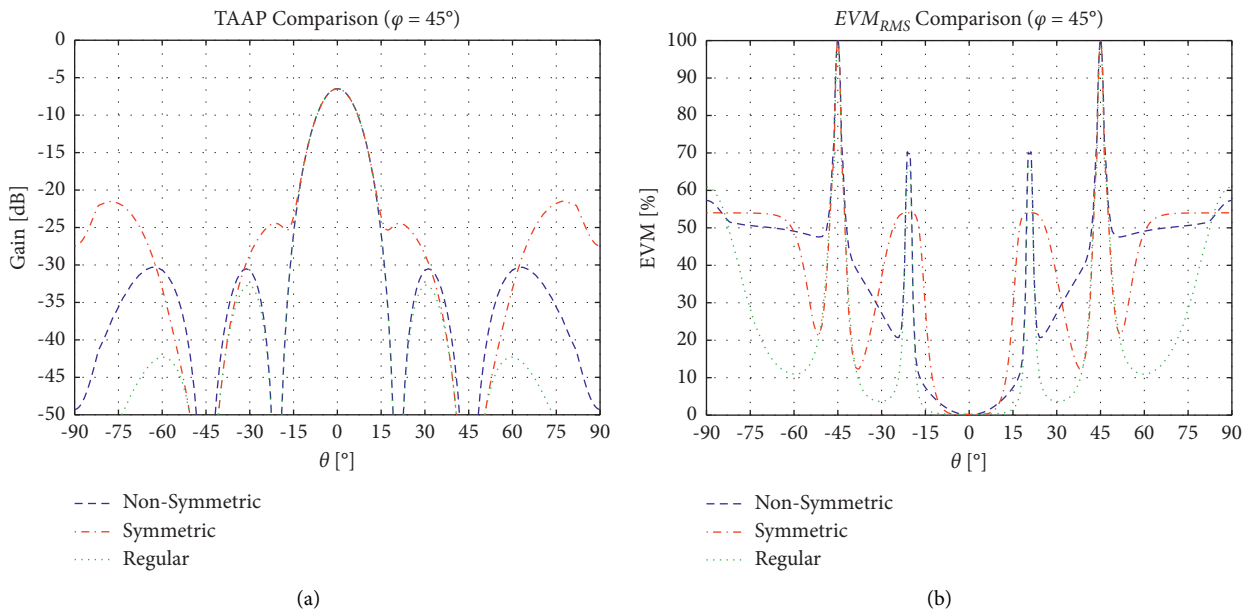

FIGURE 6: TAAP and EVM performance comparison between the regular array and the outspacing symmetric and nonsymmetric configuration at the cross section: $\varphi = 45^\circ$, $K = L = 8$, $d_x = d_y = \lambda_0/2$, $C/N = 50\ dB$, transmitted signal is QAM16, and a cos θ element power pattern is used. (a) Time average array pattern. (b) EVM.

2.6. Scanning Scenarios of Arrays. Multiple beamforming scenarios exist ranging from wide-angle scanning in base stations for 5G/6G wireless communications to limited-scan scenarios in point-to-point communications, where only small beam adaptions are required to compensate mechanical and weather effects [10]. Both outspacing configurations shown in Figures 4(a) and 5(a) are configured for limited-scan applications and, as a consequence, have a relative poor scan performance due to the appearance of grating lobes, when used in a wide-angle scan scenario as compared to traditional (nonoutspacing) dense arrays with an element spacing of $(\lambda_0/2)$. The nonsymmetric configuration, which has the best scan performance, has a grating-lobe-free scan range of $\pm 20^\circ$ and a scan loss of 0.3 dB. The relative small grating-lobe-free scan range is caused by the usage of two elements for the reconstruction of the original signal, resulting in an effective element spacing which is larger than $(\lambda_0/2)$. Reduction of the element spacing also increases the grating-lobe-free scan range, possibly at the expense of more mutual coupling. As an example, the scan performance of the nonsymmetric configuration with element spacing of $(\lambda_0/3)$ is investigated. The TAAP and EVM, when scanned to $\theta_0 = 45^\circ$ and $\phi_0 = 0^\circ$, are shown in Figure 7. As expected, no grating lobes are visible and the EVM is shifted accordingly to the desired scan angle. Note that we ignored the effect of mutual coupling. The effect of mutual coupling in such an array will impact the active impedance and associated overall efficiency of the outspacing concept (see also Section 4). Examples of closely spaced element arrays can be found in [16]. Other options to further explore are the use of triangular or irregular array grids [17]. The study on the limitations and opportunities of wide-scan

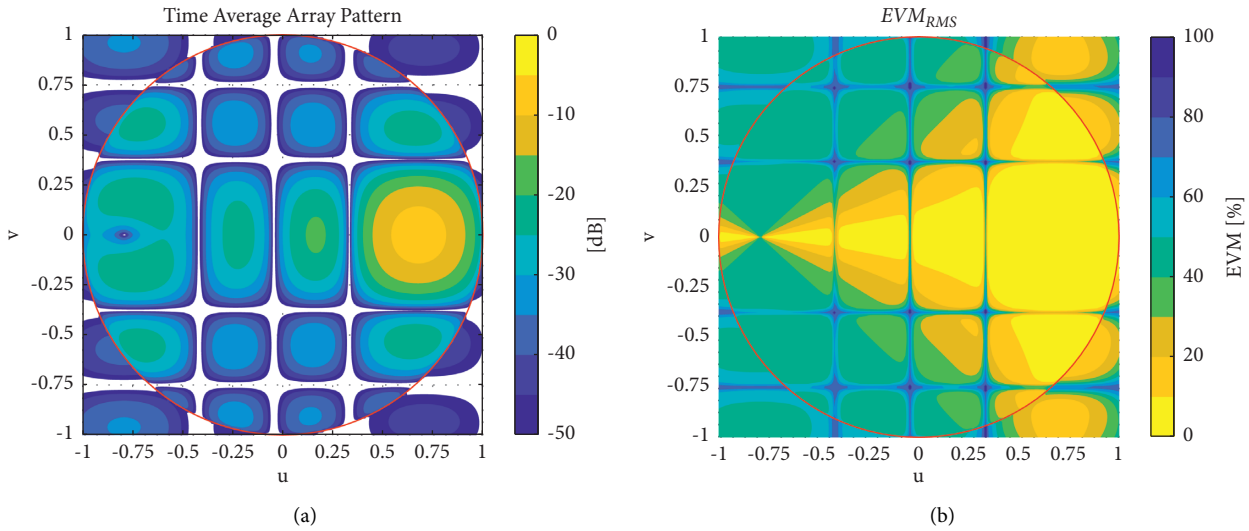

Figure 7: Scan performance of a nonsymmetric outspacing configuration with reduced element spacing with scanning to $\theta_0 = 45^\circ$ and $\phi_0 = 0^\circ$: $K = L = 8$, $d_x = d_y = (\lambda_0/3)$, $C/N = 50$ dB, the transmitted signal is QAM16, and a cos θ element power pattern is used. (a) Time average array pattern. (b) EVM.

outspacing arrays is a topic for future research and is not included in this paper.

3. Demonstrator and Experimental Verification

A proof of concept is designed to verify the underlying principles of the outspacing concept. For example, the influence of mutual coupling between elements can be significant on the performance of the outspacing array and could potentially make the concept unusable when too much signal distortion is introduced. Therefore, the demonstrator is used to investigate the effect of the active reflection coefficient. Furthermore, the embedded element patterns are investigated. In addition, over-the-air (OTA) testing is done to measure the system-level parameters of the outspacing concept.

3.1. Demonstrator Design. A planar patch antenna array is designed to experimentally verify the behavior of an outspacing array. An equally spaced 4×4 array operating at 2.4 GHz is chosen for this proof-of-concept array to reduce technology-related risks in the realization of the demonstrator and to focus on the verification of the outspacing concept first. In addition, this frequency band is close to the new 5G 3.5 GHz band, where our concept could also be applied. The planar array consists of sixteen probe-fed patch antennas of 31.3×31.3 mm. The probe is realized by a via, which is directly connected to the center pin of a surface mount SMA connector. The elements are spaced at 0.5λ distance, placed on a 1.524 mm-thick RO4350B™ substrate of 250×250 mm. The planar array is designed in CST [18] and can be seen in Figure 8.

3.2. Active Reflection Coefficient. Mutual coupling between the array elements has, in general, a negative impact on the array performance. To investigate the impact of mutual coupling on the performance of the outspacing array, the active reflection coefficient [17], Γ_j^{act}, is used, which can be calculated by

$$\Gamma_j^{\text{act}} = \frac{1}{A_j O_j} \sum_{i=1}^{K \times L} S_{ij} A_i O_i, \tag{7}$$

where S_{ij} represents the scattering parameter between array elements j and i. Scattering parameters $S_{1,1}$ to $S_{1,16}$ are measured and compared with a simulation model, which showed negligible difference, and therefore, the simulated scattering parameters are used for analysis. Γ_j^{act} of all sixteen elements of the 4×4 array is calculated in the nonsymmetric and symmetric configuration, with the outspacing angle ψ as variable. The results are shown in Figure 9. The four center elements of the array are marked with a square marker, and the color of the trace refers to the outspacing polarity (β_j). The difference between both configurations is substantial. Both configurations perform similar at $\psi = 0$, but at larger outspacing angles, the active reflection coefficient stays fairly constant for the symmetric configuration, whereas the active reflection coefficient of the nonsymmetric configuration increases significantly. The reason for the major difference is the outspacing polarity of the neighboring elements. For the nonsymmetric configuration, the four closest elements always have an opposite outspacing polarity compared to the center element. The four closest elements of the symmetric configuration have a balanced polarity (two for each outspacing polarity), resulting in partly cancellation of the mutual coupling effect. When the arrays are used for beam steering, the results will significantly change, especially for the nonsymmetric configuration. Although the nonsymmetric configuration shows large variation over outspacing angle, this effect could potentially be used for efficiency enhancement, comparable to the concept of Chireix [19]. In Section 4, a more in-depth analysis is performed on the outspacing efficiency and possible improvements. When a

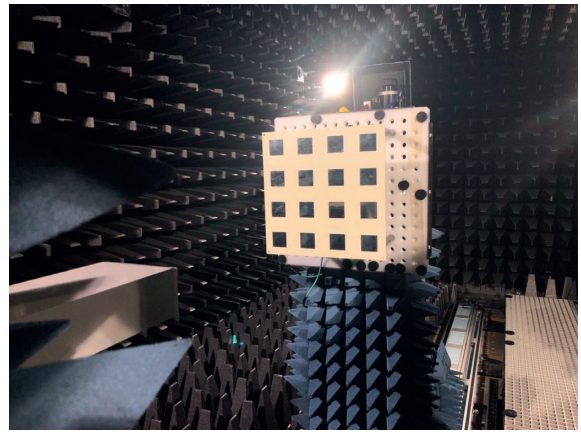

Figure 8: 4 × 4 array used for demonstration of the outspacing concept in the anechoic test chamber.

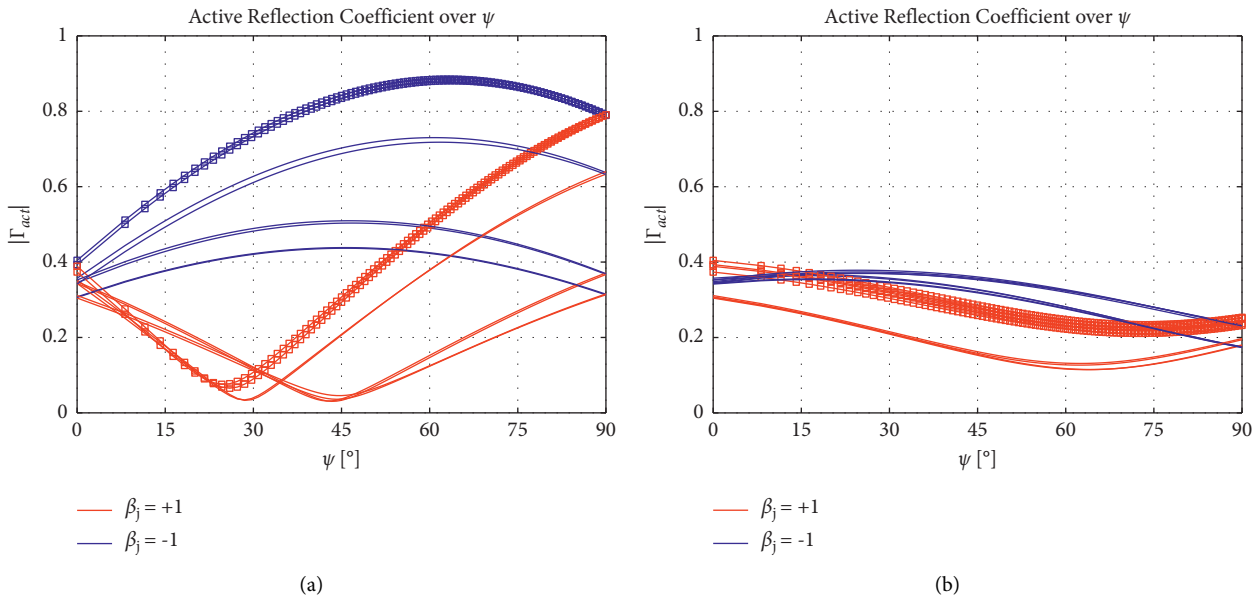

Figure 9: Active reflection coefficient over outspacing angle ψ of the designed 4 × 4 array without beam steering in the nonsymmetrical and symmetrical outspacing configuration. The marked traces refer to the four center elements and the color to the outspacing polarity (β_j). (a) Nonsymmetric configuration. (b) Symmetric configuration.

very constant impedance is required, the symmetric configuration is the preferred configuration.

3.3. The Embedded Element Pattern. The embedded element patterns of all sixteen elements are measured in a far-field anechoic test facility versus θ and φ. The normalized measurement results are shown in Figure 10. The measured embedded element patterns are included in our overall outspacing array model to check the impact of nonideal elements (shown in Figure 11). No normalization is performed between the elements when used in the outspacing array model. The PSLL is equal to −13 dB and the ASLL is equal to −20.1 dB compared to −16.6 dB and −22.6 dB, respectively, for a cos θ element power pattern, where the average main beam level is equal to −6.5 dB. The reduction in sidelobe performance is caused by the low number of elements and the impact of mutual coupling. The realized TAAP cross sections in Figure 11(a) show a very small difference between the TAAP including embedded element pattern compared to the pattern realized with a cos θ element power pattern.

3.4. Over-the-Air (OTA) Testing of Outspacing Performance. The system-level outspacing measurement setup is shown in Figure 12. The outspacing signals are generated and analyzed by a National Instruments (NI) PXI chassis, consisting of two FlexRIO transceiver cards and controlled by LabVIEW. The FlexRIO card generates the constant envelope outspaced signals ($O(-\beta)$ and $O(+\beta)$) in in-phase and quadrature (IQ) format, modulated at dc. The modulators (MAX2022) upconvert the IQ outspacing signals to the desired carrier frequency of 2.4 GHz. The two outspaced signals are split into two pairs of eight identical outspaced signals by a power

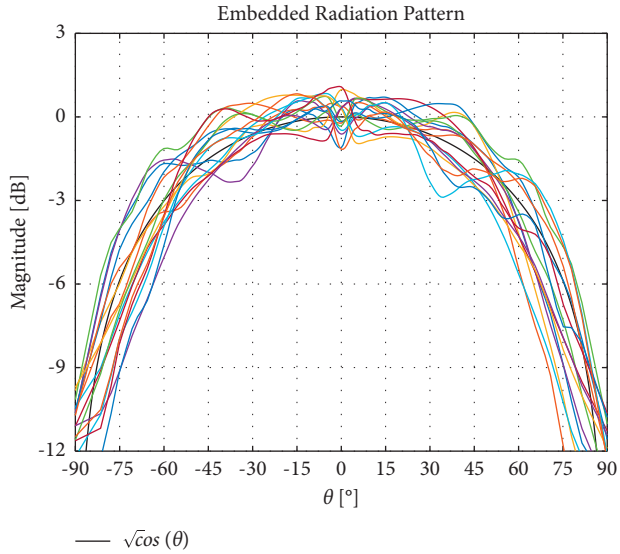

Figure 10: Normalized embedded element patterns of the designed 4×4 array measured in the anechoic test facility at 2.4 GHz.

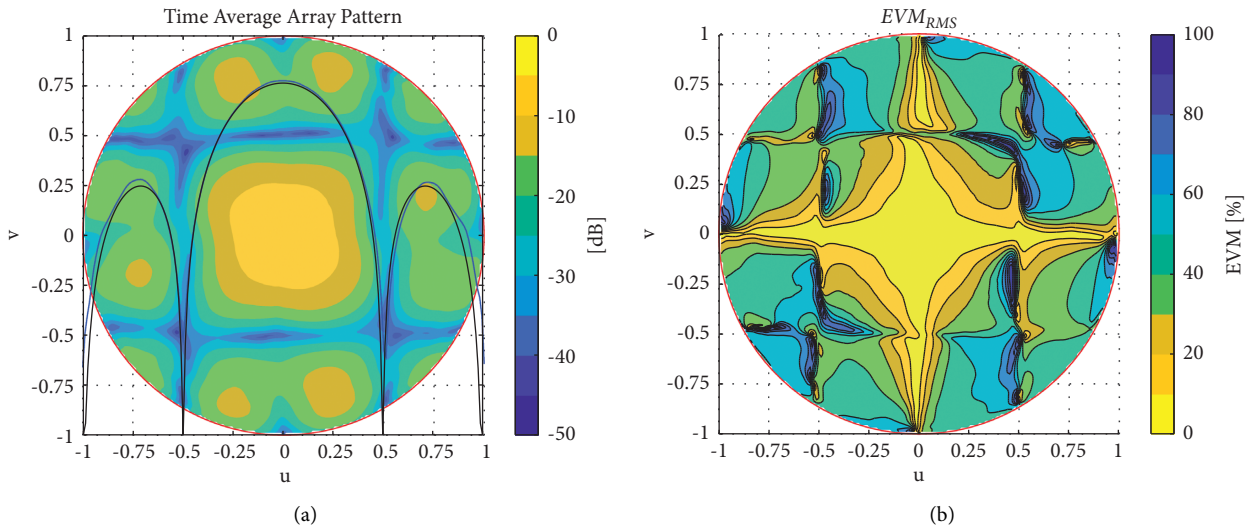

Figure 11: Nonsymmetric array performance including the measured demonstrator embedded element patterns: $K = L = 4$ and $d_x = d_y = (\lambda_0/2)$. (a) Time average array pattern, where black and blue traces are cross sections at $v = 0$ with $\sqrt{\cos\theta}$ and embedded element pattern, respectively. (b) EVM.

splitter (Mini-Circuits ZN8PD-642W-S+) which is located close to the array in the anechoic chamber, as shown in Figure 8. The two pairs of eight outspaced signals are fed to the phased array in the desired configuration. No complex excitation coefficient A_j is applied to each element, which greatly simplifies the measurement setup. The transmitted signal is measured with an open-ended waveguide probe (WR430) located in the far field. The received complex modulated signal is connected to a spectrum analyzer (Keysight N9918 B) and demodulator (MAX2022). The demodulator is used to downconvert the complex modulated signal to dc, such that it can be analyzed by the FlexRIO transceiver. The spectrum analyzer is used to measure the channel power, and from this, the radiation pattern is determined. In LabVIEW, the signal is analyzed and the EVM is determined. Furthermore, the LabVIEW program can perform a calibration for reducing offset, gain, and phase errors, improving the signal quality.

The outspacing array is rotated with a step-size of 5° over θ in the $\varphi = 0°$ plane. At each angular position, the radiated power and EVM are measured. The measurement results are shown in Figure 13. The measured TAAP is very comparable to the modeled TAAP including embedded element pattern, especially within $|\theta| = 60°$. Outside $|\theta| = 60°$, the measured results deviate slightly from the simulations, which is mainly due to the effect of supporting structures used to mount the demonstrator on the positioner. The measured EVM is also very comparable to the simulated EVM, except for the high peak at $\theta = 70°$, which can also be explained by the effect of supporting structures and other measurement errors. The EVM within the 3 dB main

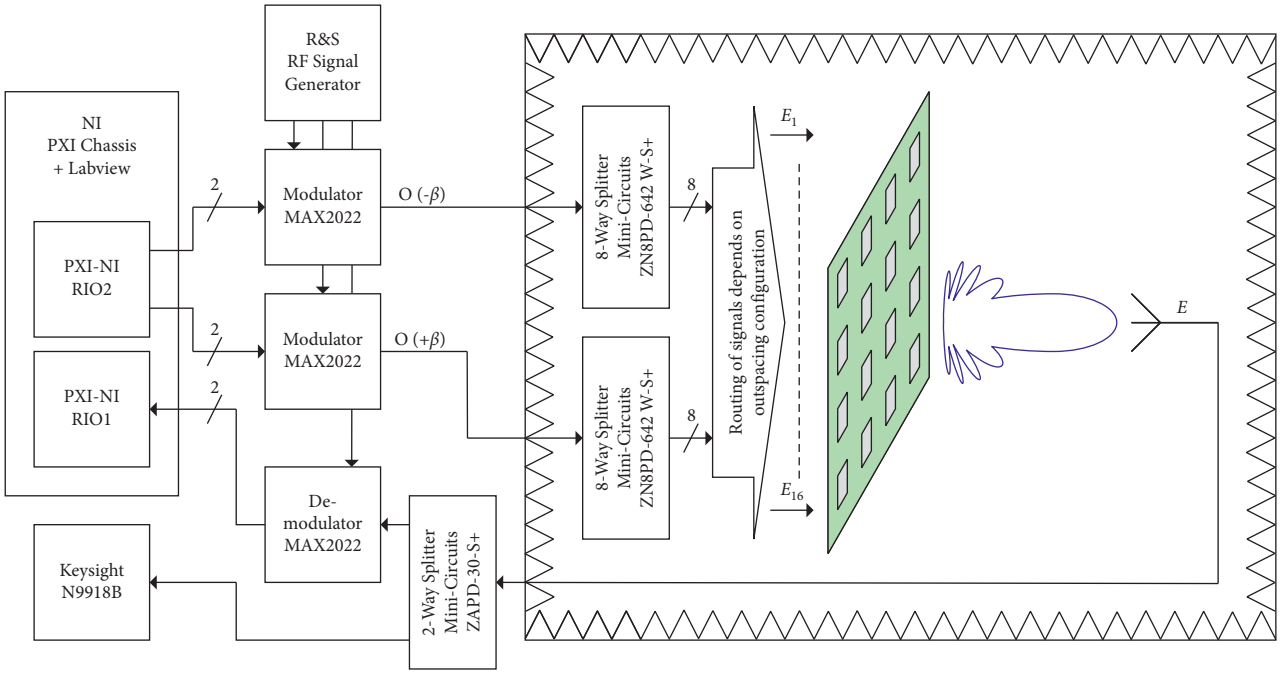

Figure 12: OTA measurement setup for measuring the outspacing behavior in an anechoic test chamber.

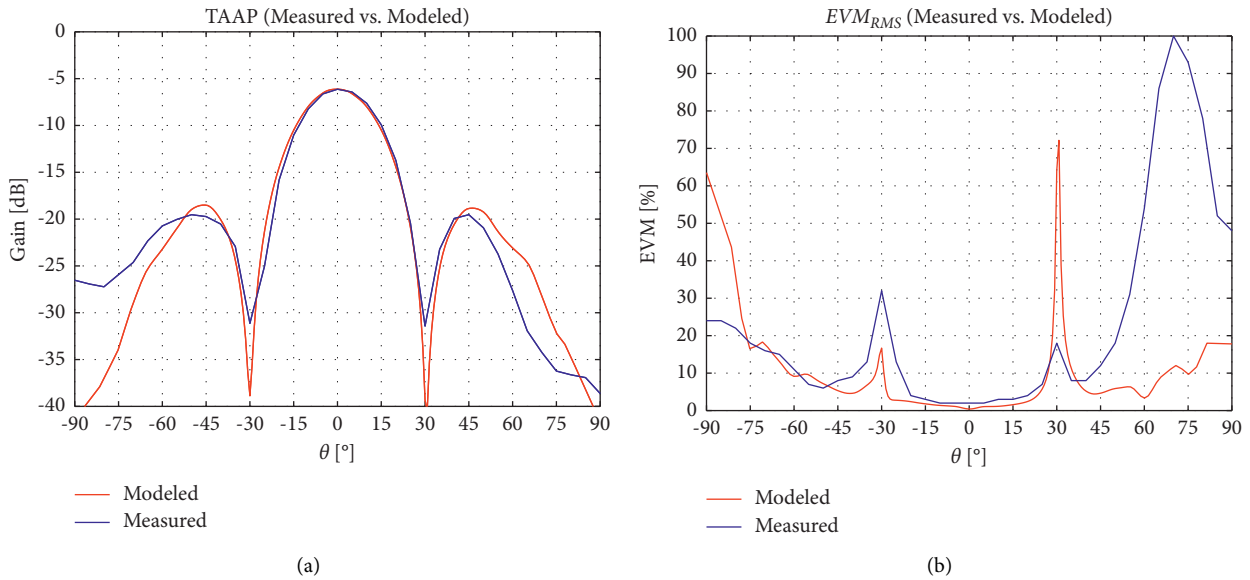

Figure 13: Demonstrator outspacing performance. The nonsymmetric configuration is measured in the anechoic chamber over the $\varphi = 0^\circ$ plane. As a reference, the modeled result including embedded element pattern is shown. $K = L = 4$, $d_x = d_y = (\lambda_0/2)$, and the transmitted signal is QAM16. (a) Time average array pattern. (b) EVM.

beam is well below 3%, which is much lower than the allowed maximum for a QAM16 signal [13].

The outspacing performance was measured at 2.4 GHz, which has a lower impact on the design and technology complexity compared to mm-wave frequencies such as 28 GHz. Note that the theoretical analysis of our concept is independent of the used frequency or application; however, at mm-wave frequencies, new challenges are introduced such as the package integration technology and the need for larger bandwidths. At mm-wave frequencies, component tolerances and thermal aspect will become much more relevant. The impact of an amplitude and phase error on the outspacing signal is already described in [3]. The advantage of the outspacing concept is that random errors per element will be partly cancelled out, making the requirements less stringent compared to a traditional LINC concept. Eventually, a regular phased array at mm-wave will also require postmanufacturing calibration [20] making the challenges

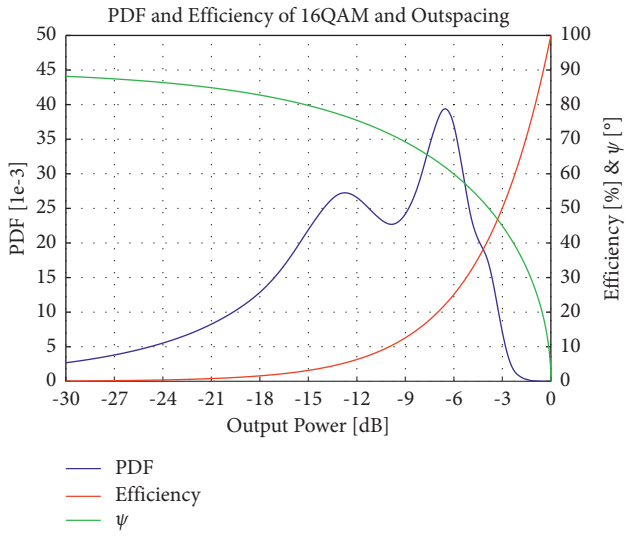

Figure 14: Probability density function of a QAM16 signal over output power, compared to the efficiency and outspacing angle ψ over output power for an isolated outspacing phased array.

not very different compared to an outspacing phased array at mm-wave.

4. Outspacing Efficiency Performance

Transmitter efficiency is a key performance indicator in modern wireless systems. The theoretical efficiency performance of the outspacing concept can be compared to an isolated outphasing concept, also known as LINC [3], assuming there is no mutual coupling between the antenna elements. In a traditional LINC system, the in-phase component is delivered to the load, where the out-phase component is dissipated in the isolation resistor of the isolated combiner, such as used in the Wilkinson power combiner. In the outspacing concept, the in-phase component is coherently summed in the main beam, whereas the out-phase component is transmitted in other directions. Without mutual coupling, due to the isolation, no load modulation occurs, resulting in a constant amplifier load. Generating constant power in a constant load, independently of the outspacing angle, results in a class-A like efficiency, which is proportional to the output power. This is graphically shown in Figure 14, where the efficiency and outspacing angle are plotted over output power. The plotted efficiency is inherent to an outspacing concept without load modulation and does not include the amplifier efficiency, which realistically is in the range of 10 – 40% for mm-wave amplifiers, depending on the technology [21]. In a regular phased array, the efficiency is mainly determined by the applied amplifier topology. When conventional linear class amplifiers, such as class-(A)B, are used in a regular phased array, it is required to operate at back-off to meet the EVM and spectral mask specifications. An improvement on the back-off efficiency can be achieved with the Doherty topology [1], but at mm-waves, the Doherty topology suffers from reduced peak and back-off efficiency due to the lossy on-chip combiner and nonideal operation [2]. In an outspacing array, the amplifiers can be optimized to operate in saturation and therewith at a higher peak efficiency, which could potentially result in an improved average efficiency when transmitting a signal with a large PAPR. As shown in Section 3.2, in practice, the mutual coupling and therewith the active reflection coefficient are significant and cannot be neglected. In the symmetric configuration, the active reflection coefficient is relatively constant, making the configuration less attractive for enhancing the efficiency by active load modulation. The active load impedance of each amplifier remains constant over the outspacing angle and, therefore, the amplifiers can be optimized for a single load point. Without active load modulation, the outspacing concept can be made very linear and well controllable, which makes it very useful for digital implementations. Because of its well-controllable behavior due to its constant load, power supply modulation is an attractive strategy for improving transmitter efficiency. A more digital way of increasing the efficiency at higher outphasing angles can be achieved by discrete supply modulation such as multilevel LINC (ML-LINC) [22] or asymmetric multilevel outphasing (AMO) [23]. For each transition between two supply levels, the outphasing angle is reset to zero, resulting in an efficiency peak. Supply modulation brings challenges when a wide bandwidth is required, such as required to comply to future wireless communication standards. Nonetheless, supply modulation could also be used to achieve amplitude tapering or EIRP modulation in case of moving user equipment.

The nonsymmetric configuration shows a very strong dependency between the outspacing angle and active reflection coefficient. This effect can potentially be used for efficiency enhancement by load modulation, like the concept of Chireix [19]. By adapting the magnitude and phase of the coupling between elements, the active reflection coefficient could be optimized such that the impedance increases at large outspacing angles. The higher load impedance at larger outspacing angles results in a reduction of the power consumption and therefore a higher drain efficiency [24]. More research is required to prove the feasibility of the efficiency enhancement in combination with an optimized mutual coupling in outspacing phased arrays.

5. Conclusion and Future Work

In this paper, the performance of outspacing planar phased arrays is discussed. New performance metrics are required such as the introduced time average array pattern (TAAP) because the well-known phased array performance metrics are insufficient. It is shown that the average and peak sidelobe level of the nonsymmetric configuration is very comparable to a regular nonoutspacing array. Furthermore, strong degradation of the EVM outside the main beam is demonstrated, which can be beneficial from a security point of view. The outspacing concept shows its largest potential in a limited-scan scenario. Next to this, wide-scan scenarios could also be considered by reducing the element spacing of the nonsymmetric configuration.

In this work, the outspacing behavior of a 4×4 phased array at 2.4 GHz is measured in the anechoic chamber. Both the TAAP and the EVM are analyzed showing a very good

agreement with theory. We have realized an EVM below 3% in the main beam of the array. The symmetric configuration has a near constant active reflection coefficient versus outspacing angle, which is attractive for achieving high linearity at the expense of efficiency. The active reflection coefficient of the nonsymmetric configuration shows a strong dependency w.r.t. outspacing angle and could potentially be used for efficiency enhancement by active load modulation.

More future work can be performed on the investigation of other outspacing configurations. The configuration of β_j and the element grid could be investigated. In addition, amplitude tapering could be used to minimize sidelobes and improve the performance. Density tapering and supply modulation are methods which could fit outspacing very well. Furthermore, the concept is demonstrated at 2.4 GHz and requires additional work to show its full potential at mm-wave frequencies. The promising results of the active reflection coefficient show large potential for achieving active load modulation by array mutual coupling, although this requires future work to prove its feasibility.

Data Availability

The data used to support the findings of the study can be obtained from the corresponding author upon request.

Conflicts of Interest

The authors declare that they have no conflicts of interest.

References

[1] W. H. Doherty, "A new high efficiency power amplifier for modulated waves," *Proceedings of the IRE*, vol. 24, no. 9, pp. 1163–1182, Sept 1936.

[2] T.-W. Li, M.-Y. Huang, and H. Wang, "Millimeter-wave continuous-mode power amplifier for 5G MIMO applications," *IEEE Transactions on Microwave Theory and Techniques*, vol. 67, no. 7, pp. 3088–3098, July 2019.

[3] D. Cox, "Linear amplification with nonlinear components," *IEEE Transactions on Communications*, vol. 22, no. 12, pp. 1942–1945, Dec 1974.

[4] E. Tollefson, B. R. Jordan, and J. D. Gaeddert, "Out-phased array linearized signaling (OPALS): a practical approach to physical layer encryption," in *Proceedings of the MILCOM 2015 - 2015 IEEE Military Communications Conference*, pp. 294–299, Tampa, FL, USA, October 2015.

[5] C. Liang and B. Razavi, "Transmitter linearization by beamforming," *IEEE Journal of Solid-State Circuits*, vol. 46, no. 9, pp. 1956–1969, Sept 2011.

[6] Y. Zhou, M. Y.-W. Chia, X. Qing, and J. Yuan, "RF spatial modulation using antenna arrays," *IEEE Transactions on Antennas and Propagation*, vol. 61, no. 10, pp. 5229–5236, Oct 2013.

[7] S. Li, T. Chi, J.-S. Park, H. T. Nguyen, and H. Wang, "A 28-GHz flip-chip packaged Chireix transmitter with on-antenna outphasing active load modulation," *IEEE Journal of Solid-State Circuits*, vol. 54, no. 5, pp. 1243–1253, 2019.

[8] A. Sayag and E. Cohen, "Comparison of over-the-air efficiency enhancement techniques in linear phased arrays," *IEEE Transactions on Microwave Theory and Techniques*, vol. 70, no. 1, pp. 685–695, 2022.

[9] B. G. M. van Ark, A. B. Smolders, and P. F. M. Smulders, "Outspacing phased arrays for mm-wave 5G base stations," in *Proceedings of the 2020 14th European Conference on Antennas and Propagation (EuCAP)*, pp. 1–5, Copenhagen, Denmark, March 2020.

[10] A. Al-Rawi, A. Dubok, M. Herben, and A. Smolders, "Point-to-point radio link variation at E-band and its effect on antenna design," pp. 913–917, 2015.

[11] A. Birafane, M. El-Asmar, A. Kouki, M. Helaoui, and F. Ghannouchi, "Analyzing LINC systems," *IEEE Microwave Magazine*, vol. 11, no. 5, pp. 59–71, 2010.

[12] M. Vigilante, E. McCune, and P. Reynaert, "To EVM or two EVMs?: an answer to the question," *IEEE Solid-State Circuits Magazine*, vol. 9, no. 3, pp. 36–39, Summer 2017.

[13] Technical Specification Group Radio Access Network, "NR; base station (BS) radio transmission and reception, 3rd generation partnership project std. 38.104," 06 2019, https://www.3gpp.org/ftp/Specs/latest/Rel-16/38_series/38104-g00.zip.

[14] S. Haykin and M. Moher, *Modern Wireless Communications*, Pearson Prentice Hall, Hoboken, NJ, USA, 2005.

[15] R. Hansen, *Phased Array Antennas*, Wiley, Hoboken, NJ, USA, 2009.

[16] B. A. Munk, *Broadband Wire Arrays*, pp. 181–213, John Wiley & Sons, Hoboken, NJ, USA, 2003.

[17] A. B. Smolders, H. J. Visser, and U. Johannsen, "Modern antennas and microwave circuits – a complete master-level course," 2020, https://arxiv.org/abs/1911.08484.

[18] "3 Dassault Systemes. CST Studio Suite," 2019, https://www.3ds.com/products-services/simulia/products/cst-studio-suite/.

[19] H. Chireix, "High power outphasing modulation," *Proceedings of the IRE*, vol. 23, no. 11, pp. 1370–1392, Nov 1935.

[20] A. van den Biggelaar, C. Vertegaal, U. Johannsen, M. Geurts, and A. Smolders, "Post-manufacturing calibration procedure for medium-sized silicon-based active phased arrays for mm-wave wireless communications," in *Proceedings of the 2020 14th European Conference on Antennas and Propagation (EuCAP)*, pp. 1–5, Copenhagen, Denmark, March 2020.

[21] H. Wang, T.-Y. Huang, N. S. Mannem et al., "Power amplifiers performance survey 2000-present," 2020, https://gems.ece.gatech.edu/PA_survey.html.

[22] Y. Chen, K. Jheng, A. Wu, H. Tsao, and B. Tzeng, "Multilevel LINC system design for wireless transmitters," in *Proceedings of the 2007 International Symposium on VLSI Design, Automation and Test (VLSI-DAT)*, pp. 1–4, Hsinchu, Taiwan, April 2007.

[23] P. A. Godoy, S. Chung, T. W. Barton, D. J. Perreault, and J. L. Dawson, "A 2.4-GHz, 27-dBm asymmetric Multilevel outphasing power amplifier in 65-nm CMOS," *IEEE Journal of Solid-State Circuits*, vol. 47, no. 10, pp. 2372–2384, 2012.

[24] M. Litchfield and T. Cappello, "The various angles of outphasing PAs: competitiveness of outphasing in efficient linear PA applications," *IEEE Microwave Magazine*, vol. 20, no. 4, pp. 135–145, April 2019.